*Int. J. Electrochem. Sci.*, 13 **(2018)** 5425 – 5432, doi: 10.20964/2018.06.13

International Journal of
ELECTROCHEMICAL
SCIENCE
www.electrochemsci.org

*Short Communication*

# Synthesis and Electrochemical Performance of $Na_{0.5}Li_{0.1}Ni_{0.2}Mn_{0.7}Mg_{0.1}O_2$ as a Cathode for Sodium-Ion Batteries

*Jin Wang*[1], *Zhaofu Zhou*[1], *Yushan Li*[1], *Meng Li*[1], *Jianqiu Deng*[1,2,*], *Qingrong Yao*[2,*], *Zhongmin Wang*[1,2], *Huaiying Zhou*[1,2]

[1] Guangxi Key Laboratory of Information Materials, Guilin University of Electronic Technology, Guangxi, Guilin 541004, China
[2] School of Materials Science and Engineering, Guilin University of Electronic Technology, Guangxi, Guilin 541004, China
[*]E-mail: jqdeng@guet.edu.cn (Jianqiu Deng), qingry96@guet.edu.cn (Qingrong Yao)

*Received:* 8 February 2018 / *Accepted:* 13 March 2018 / *Published:* 10 May 2018

Exploring ideal cathode materials with low cost and good electrochemical performance is the key issue for development of sodium ion batteries. Herein, P2-type layered $Na_{0.5}Li_{0.1}Ni_{0.2}Mn_{0.7}Mg_{0.1}O_2$ is synthesized by a facile self-propagating combustion method. The sample makes up of plate-like structured particles with high crystallinity. A high specific capacity of 157 mAh $g^{-1}$ at 0.2 C and good rate capability can be achieved in a voltage range of 1.5–4.6 V. The stable cycle performance is also delivered in a narrow voltage range of 2.0–4.0 V, indicating that $Na_{0.5}Li_{0.1}Ni_{0.2}Mn_{0.7}Mg_{0.1}O_2$ is a promising cathode material for sodium ion batteries.

**Keywords:** Sodium ion batteries; Cathode; P2-type layered oxide; Self-propagating combustion method.

## 1. INTRODUCTION

The development of lithium-ion batteries (LIBs) during the last three decades is so fast that they have dominated the market of portable electronic devices. However, cost and service life of LIBs are issues to limit their applications in large-scale electric energy storage [1]. As an alternative, sodium-ion batteries (SIBs) have attracted wide attention due to the natural abundance and low cost of Na resources [2-3].

The overall performance of SIBs relies on the development of high-performance cathode materials. Recently, various materials such as layered oxides, polyanionic compounds, organic compounds, and prussian blue analogues have been reported as the potential cathodes for SIBs [4]. Among them, sodium transition metal layered oxides, $Na_{1-x}MO_2$ (M: transition metals), exhibit various advantages, including stable structure, good electrochemical performance, and ease of synthesis [5]. P2-type sodium manganese-based layered oxides have been regarded as an attractive candidate than O3- and P3-type layered oxides for SIBs, due to their high capacity and operating potential. For instance, P2-$Na_{0.5}Ni_{0.25}Mn_{0.75}O_2$ cathode could exhibit a high capacity of 210 mAh $g^{-1}$ at 0.1 C [6]. However, the capacity fades rapidly due to the P2-O2 phase transformation in a wide voltage range. To achieve better cycling stability of P2-type manganese-based oxides, the substitution of Li, Mg or other metal elements such as Cu and Ti, has been carried out by many research groups to suppress the P2-O2 phase transition, and improve the structural stability [7-10].

In this work, P2-type $Na_{0.5}Li_{0.1}Ni_{0.2}Mn_{0.7}Mg_{0.1}O_2$ was prepared by a self-propagating combustion method. The effect of the operating voltage range on electrochemical performance of the cathode material was evaluated in detail. Although the capacity of the cathode material is relatively low (80 mAh $g^{-1}$), a high capacity retention of 92.1% over 80 cycles can be achieved in a voltage range of 2.0–4.0 V.

## 2. EXPERIMENTAL

### *2.1 Synthesis of Materials*

P2-$Na_{0.5}Li_{0.1}Ni_{0.2}Mn_{0.7}Mg_{0.1}O_2$ was synthesized via a self-propagating combustion method. Firstly, stoichiometric amounts of $Na_2CO_3$, $LiOH{\cdot}H_2O$, $Mn(CH_3COO)_2{\cdot}4H_2O$, $Ni(CH_3COO)_2{\cdot}4H_2O$, Mg $(CH_3COO)_2{\cdot}4H_2O$, and citric acid were dissolved in deionized water to form a mixed solution. The molar ratio of citric acid to metal ions was 1:3. The excess of 5 mol% Na was used to compensate for the volatilization of Na during calcination. The mixed solution was kept at 80 $^oC$ for 6 h to form a homogeneous sol and then was dried at 150 $^oC$ under vacuum for 24 h. The dried precursors were finally calcined at 900 $^oC$ for 12 h, and quenched to room temperature. The products were ground and immediately moved into a glove box filled with argon.

### *2.2 Materials Characterization*

X-ray diffraction pattern of the sample was collected on a PIXcel$^{3D}$ X-ray diffractometer with a nonmonochromated Cu Kα X-ray source in a range of 10–80°. The crystal structure was refined by the Rietveld method using the Fullprof software. The X-ray photoelectron spectroscopy (XPS) spectra were recorded on an ESCALAB 250Xi spectrometer (ThermoFisher Scientific, UK) equipped with monochromatic Al Kα radiation. The morphology of the sample was examined using field emission scanning electron microscopy (FE-SEM, FEI Quanta 450 FEG).

*2.3 Electrochemical Measurements*

The working electrodes were prepared by mixing the active materials (70 wt%), acetylene black (20 wt%), and polyvinylidene fluoride (PVDF, 10 wt%) in N-methyl-2-Pyrrolidone (NMP). The slurry was coated onto an Al foil using a film-coating machine and dried at 120 $^{o}$C for 10 h under vacuum condition to remove the solvent. The sheet was punched into discs, and pressed at 5 MPa prior to battery assembly. The active material loading was about 2.0–3.0 mg cm$^2$. The 2032-type coin cells were assembled with a sodium plate as a counter electrode, 0.8 M $NaPF_6$ in PC as an electrolyte, and a glass fiber as a separator in an argon-filled glove box. The charge and discharge tests were carried out on a Land battery test system (Wuhan, China) at room temperature. Cyclic voltammetry (CV) and electrochemical impedance spectroscopy (EIS) were performed on a Solartron electrochemical workstation.

## 3. RESULTS AND DISCUSSION

*3.1 Structural characterization*

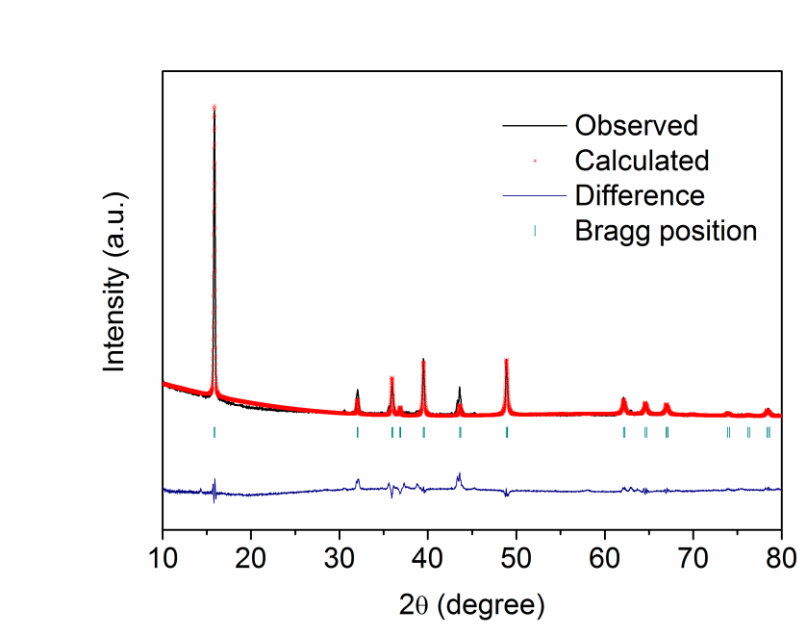


**Figure 1.** XRD pattern of $Na_{0.5}Li_{0.1}Ni_{0.2}Mn_{0.7}Mg_{0.1}O_2$.

Figure 1 shows the XRD pattern of the $Na_{0.5}Li_{0.1}Ni_{0.2}Mn_{0.7}Mg_{0.1}O_2$ sample with high crystallinity. According to the pattern, all diffraction peaks can be indexed to a hexagonal layered structure with the $P6_3/mmc$ space group (JCPDS No: 00-027-0751). The diffraction peaks of impure phase are not observed in the XRD pattern, indicating that the co-doping of Li and Mg ions does not change the crystal structure of the sample. The lattice parameters determined by Rietveld refinement are a = 2.8846 Å and c = 11.1752 Å. Compared to the lattice parameters reported in $Na_{0.6}MnO_2$ [11],

smaller c value is induced by the substitution of the smaller ionic radius of Li ions. From the Rietveld refinement analysis, the parameters $R_{wp}$, $R_p$ and $\chi^2$ are 17.3%, 13.1% and 12.7%, respectively, which represents the satisfactory quality. The co-existence of Li and Mg ions in $Na_{0.5}Li_{0.1}Ni_{0.2}Mn_{0.7}Mg_{0.1}O_2$ is expected to enhance the cycling stability of sodium manganese-based cathode materials. Figure 2 presents FE-SEM images of the $Na_{0.5}Li_{0.1}Ni_{0.2}Mn_{0.7}Mg_{0.1}O_2$ sample. The sample consists of plate-like structured primary particles, which is in good agreement with the layered structure of this material. The large secondary aggregates with a particle size range of 1–30 μm are observed in the SEM images, which is due to the high-temperature calcination at 900 $^oC$.

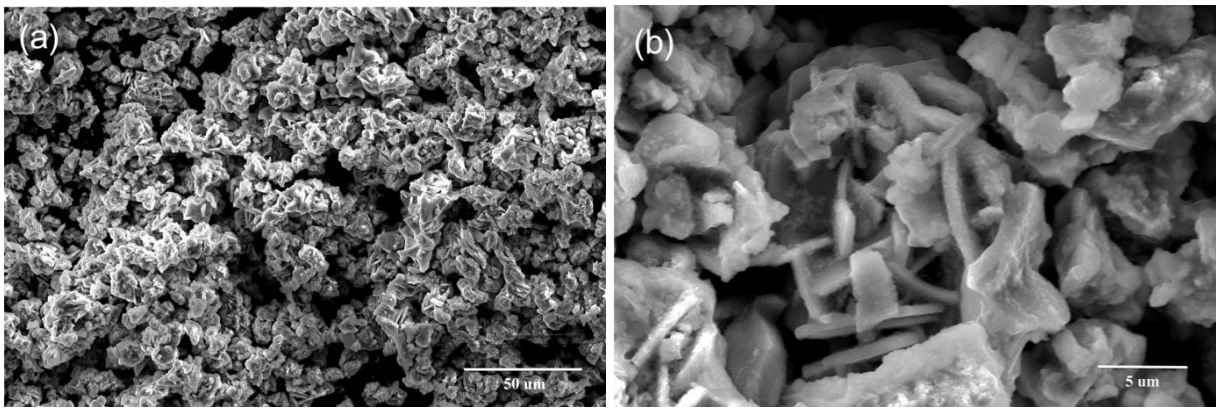


**Figure 2.** FE-SEM images of $Na_{0.5}Li_{0.1}Ni_{0.2}Mn_{0.7}Mg_{0.1}O_2$ sample.

The oxidation states of transition metals of the as-prepared sample were analyzed by the X-ray photoelectron spectroscopy (XPS), as shown in Figure 3. The Mn $2p_{3/2}$ peak of $Na_{0.5}Li_{0.1}Ni_{0.2}Mn_{0.7}Mg_{0.1}O_2$ was deconvoluted into two peaks at 642.5 and 642.1 eV, corresponding to $Mn^{4+}$ and $Mn^{3+}$, respectively. The binding energy peak positions are good agreement with the results reported in $LiMn_{1.5}Ni_{0.5}O_4$ [12] and $Na_{0.67}[Mg_{0.28}Mn_{0.72}]O_2$ [13].

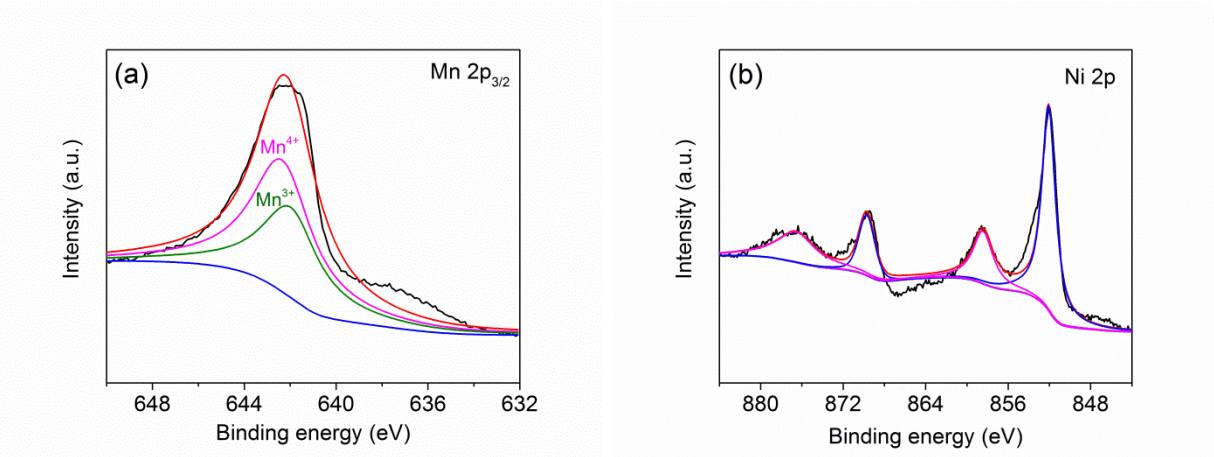


**Figure 3.** XPS spectra of Mn $2p_{3/2}$ (a) and Ni 2p (b) for $Na_{0.5}Li_{0.1}Ni_{0.2}Mn_{0.7}Mg_{0.1}O_2$.

Two characteristic peaks located at 871.65 and 853.78 eV in the Ni 2p XPS spectrum (Fig. 3b) can be attributed to Ni $2p_{1/2}$ and Ni $2p_{3/2}$ of the $Ni^{2+}$ oxidation state. Two minor peaks at 858.4 and

876.7 eV are assigned to Ni 2p of $Ni^{3+}$ oxidation state. The binding energy for the center of Ni $2p_{3/2}$ peak at about 854 eV has reported in previous works [9, 10].

### *3.2 Electrochemical studies*

The electrochemical properties of the sample were characterized by galvanostatic charge−discharge tests, cyclic voltammetry and electrochemical impedance measurements. The initial three CV curves of $Na_{0.5}Li_{0.1}Ni_{0.2}Mn_{0.7}Mg_{0.1}O_2$ sample are depicted in Figure 4a. The redox peaks at around 1.87/1.73 V is related to the redox reactions of the $Mn^{4+}/Mn^{3+}$ pair [14]. And the three couples of peaks located at the voltage range from 3.0 to 3.8 V are attributed to the $Ni^{2+}/Ni^{4+}$ redox reaction, while the oxidation/reduction peaks at around 4.03/4.26 V are ascribed to the P2-O2 phase transition during the Na-ion insertion/desertion processes [15].

From Fig. 4b, $Na_{0.5}Li_{0.1}Ni_{0.2}Mn_{0.7}Mg_{0.1}O_2$ displays a relatively good rate capability in a voltage range of 1.5–4.6 V. The discharge capacities are 148.2, 119.6, 97.3, 76.2, and 63.8 mAh $g^{-1}$ at various rates of 0.2, 0.4, 1, 2 and 4 C (1C=120 mA $g^{-1}$), respectively. When the current density comes back to 0.2 C, the capacity can recover to 145.8 mAh $g^{-1}$, indicating a good electrochemical reversibility. The good rate capability suggests that the co-doping of lithium and magnesium not only can stabilize the P2-type structure but also can enhance sodium ion diffusion kinetics. Billaud et al. have reported that Mg doping can increase the concentration of $Mn^{4+}$ and suppress Jahn-Teller distortion of P2-$Na_{2/3}[Mn_{1-x}Mg_x]O_2$, then enhance the electrochemical performance [7]. Lithium substitution for Ti in $Na_{0.67}Mn_{0.55}Ni_{0.25}Ti_{0.2}O_2$ can improve both the electronic conductivity and the sodium-ion diffusion coefficient, and lead to a notable improvement in the rate capability accordingly [9].

Fig. 4c shows the first two charge/discharge profiles of $Na_{0.5}Li_{0.1}Ni_{0.2}Mn_{0.7}Mg_{0.1}O_2$ sample cycled between 1.5 and 4.6 V versus $Na^+/Na$ at 0.2 C. The profiles show five plateaus, corresponding to five pairs of redox peaks in CV curves. The initial discharge capacity is 157.0 mAh $g^{-1}$, which is comparable to that of the previous reported materials, as summarized in Table 1. However, the sample exhibits a poor cycling stability, and a capacity retention is just 63% after 50 cycles (Fig. 4d). The rapid capacity fading may be attributed to P2-O2 phase transition in the wide voltage range of 1.5–4.6 V [15].

In order to eliminate the adverse effects of P2-O2 phase transition and the Jahn-Teller distortion of $Mn^{3+}$ ions on cycling stability, we have further investigated the cycle performance of the sample in a narrow voltage range of 2.0–4.0 V, as shown in Fig. 4e. Although the discharge capacity is 80 mAh $g^{-1}$ in the first cycle, it fades slowly over 80 cycles, indicating that the cycle performance can be improved by suppressing the irreversible P2-O2 phase transition at 4.2 V. In addition, the negative effect of the Jahn-Teller distortion of $Mn^{3+}$ ions could be inhibited in the voltage range of 2.0–4.0 V, in favour of enhancing of cycling stability.

To further evaluate the kinetic properties, electrochemical impedance spectroscopy (EIS) spectrum of the $Na_{0.5}Li_{0.1}Ni_{0.2}Mn_{0.7}Mg_{0.1}O_2$ sample was tested in fully discharge state of the cell after 50 cycles. The AC voltage amplitude of 5 mV was used in the frequency range of 100 KHz–10 mHz. EIS spectrum of the sample shown in Fig. 4f is composed of two depressed semicircles and a straight

slop line. The depressed semicircle in the high-frequency region is attributed to the transport of sodium ions through the surface layer [19]. The semicircle at the medium-frequency region and the straight slope line in the low-frequency region correspond to charge transfer resistance and Warburg impedance, respectively.

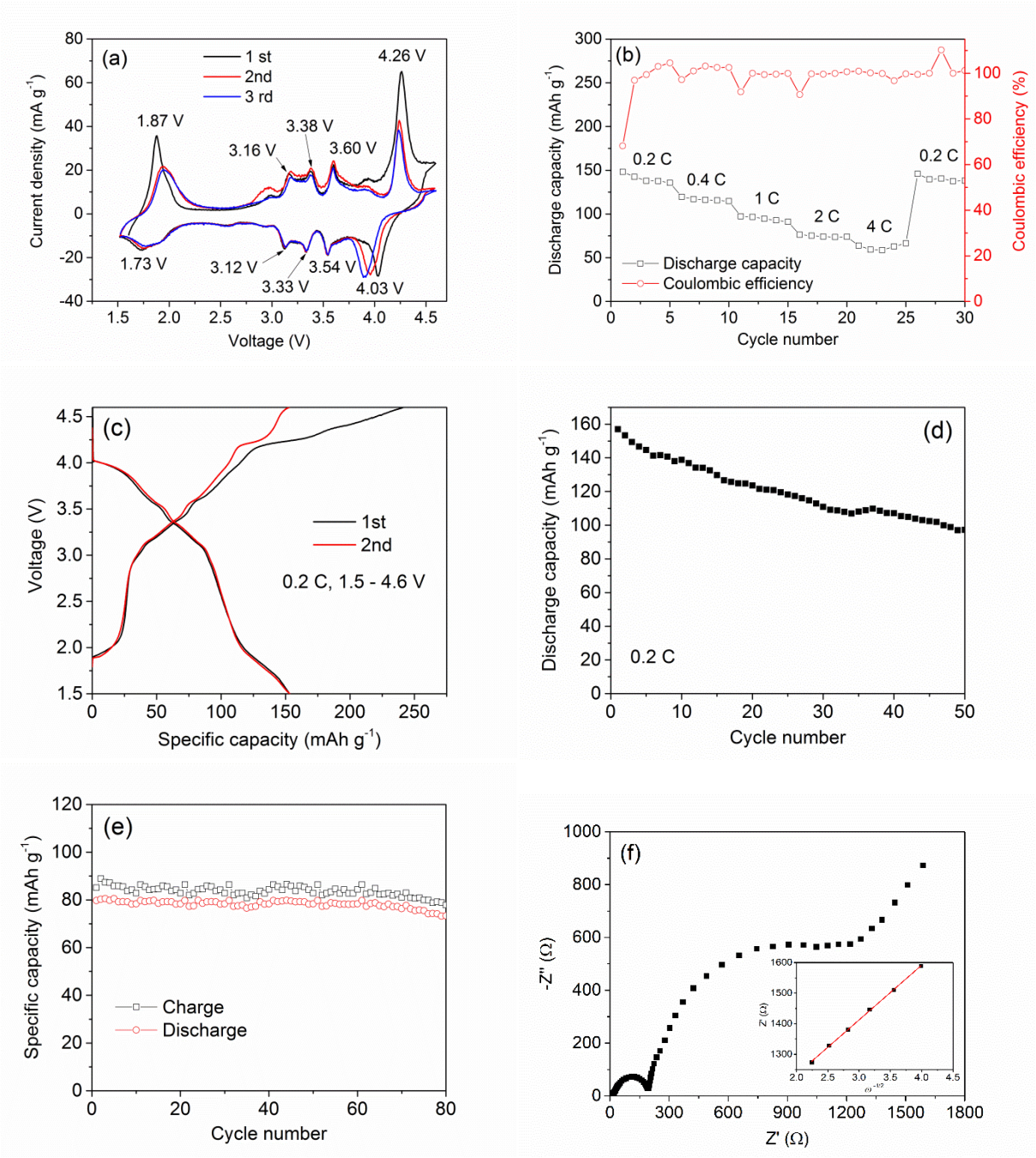


**Figure 4.** Electrochemical properties of $Na_{0.5}Li_{0.1}Ni_{0.2}Mn_{0.7}Mg_{0.1}O_2$ sample. (a) The initial three cyclic voltammograms tested between 1.5 and 4.6 V at a scan rate of 0.1 mV $s^{-1}$. (b) Rate capability. (c) Galvanostatic charge/discharge curves. (d) Cycle performance at 0.2 C in a voltage range of 1.5–4.6 V. (e) Cycle performance at 0.2 C in a voltage range of 2.0–4.0 V. (f) EIS spectrum of the sample after 50 cycles.

**Table 1.** A comparison of electrochemical performance of $Na_{0.5}Li_{0.1}Ni_{0.2}Mn_{0.7}Mg_{0.1}O_2$ with previous reported cathode materials.

| Materials | Reversible capacity (mAh $g^{-1}$) | Capacity retention | Current density (mA $g^{-1}$) | Voltage range (V) | Ref. |
|---|---|---|---|---|---|
| $Na_{0.75}Mn_{0.55}Ni_{0.25}Co_{0.05}Fe_{0.10}Zr_{0.05}O_2$ | 143 | 74% (100) | 12 | 1.5–4.2 | [16] |
| $Na_{0.80}Li_{0.12}Ni_{0.22}Mn_{0.66}O_2$ | 133 | 91% (50) | 12 | 2.0–4.4 | [17] |
| $Na_{2/3}Ni_{1/3}Mn_{1/2}Ti_{1/6}O_2$ | 127 | 94% (10) | 12 | 2.5–4.35 | [18] |
| $Na_{0.5}Li_{0.1}Ni_{0.2}Mn_{0.7}Mg_{0.1}O_2$ | 157 | 63% (50) | 24 | 1.5–4.6 | This work |
| | 80 | 92% (80) | 24 | 2.0–4.0 | |

Sodium ion diffusion coefficient can be calculated by the following formula [20]:

$$D = \frac{2R^2T^2}{A^2n^4F^4C^2\sigma^2} \quad (1)$$

$$Z_w = \sigma(1-j)\omega^{-1/2} \quad (2)$$

where $R$ is the gas constant, $T$ is the absolute temperature, $A$ is the surface area of the electrode, $n$ is the number of electrons per species during oxidization, $F$ is Faraday's constant, $C$ is the concentration of sodium ions in the cathode materials, and $\sigma$ is the Warburg factor obtained from the linear relationship between the real impedance ($Z'$) and $\omega^{-1/2}$ in the low-frequency region (the inset in Fig. 4f). The calculated sodium ion diffusion coefficient is $3.19\times10^{-13}$ $cm^2$ $s^{-1}$, indicating that this material can achieve high rate capability. The sodium ion diffusion coefficient in this work is comparable with that of P2-type $Na_{0.53}MnO_2$ nanorods ($5.21\times10^{-14}$ $cm^2$ $s^{-1}$) [21].

## 4. CONCLUSIONS

P2-type $Na_{0.5}Li_{0.1}Ni_{0.2}Mn_{0.7}Mg_{0.1}O_2$ has been successfully prepared by a self-propagating combustion method. The sample delivers a high specific capacity of 157 mAh $g^{-1}$ at 0.2 C and good rate capability in a voltage range of 1.5–4.6 V. However, the capacity fades rapidly owing to the P2-O2 phase transition during cycling, causing irreversible capacity loss. The stable cycle performance can be achieved by testing in a narrow voltage range of 2.0–4.0 V. The results demonstrate that $Na_{0.5}Li_{0.1}Ni_{0.2}Mn_{0.7}Mg_{0.1}O_2$ is a promising cathode material for sodium ion batteries.

ACKNOWLEDGEMENTS
This work was funded by the National Natural Science Foundation of China (No. 51661009) and was jointly sponsored by Guangxi Key Laboratory of Information Materials (Guilin University of Electronic Technology), P.R. China (Project No. 171006-Z).

## References

1. C. Fang, Y. Huang, W. Zhang, J. Han, Z. Deng, Y. Cao and H. Yang, *Adv. Energy Mater.*, 6 (2016) 1501727.

2. K. Kubota and S. Komaba, *J. Electrochem. Soc.*, 162 (2015) A2538-A2550.
3. C. Huang, Z. Zuo, J. Deng, Q. Yao, Z. Wang and H. Zhou, *Int. J. Electrochem. Sci.*, 12 (2017) 9456-9464.
4. J.Y. Hwang, S.T. Myung and Y.K. Sun, *Chem. Soc. Rev.*, 46 (2017) 3529-3614.
5. M.H. Han, E. Gonzalo, G. Singha and T. Rojo, *Energy Environ. Sci.*, 8 (2015) 81-102.
6. P. Manikandan, D. Ramasubramonian and M.M. Shaijumon, *Electrochim. Acta*, 206 (2016) 199-206.
7. J. Billaud, G. Singh, A.R. Armstrong, E. Gonzalo, V. Roddatis, M. Armand, T. Rojo and P.G. Bruce, *Energy Environ. Sci.*, 7 (2014) 1387-1391.
8. W. Kang, Z. Zhang, P.K. Lee, T.W. Ng, W. Li, Y. Tang, W. Zhang, C.S. Lee and D.Y.W. Yu. *J. Mater. Chem. A*, 3 (2015) 22846-22852.
9. Z.Y. Li, J. Zhang, R. Gao, H. Zhang, L. Zheng, Z. Hu and X. Liu, *J. Phys. Chem. C*, 120 (2016) 9007-9016.
10. H.V. Ramasamy, K. Kaliyappan, R. Thangavel, V. Aravindan, K. Kang, D.U. Kim, Y. Park, X. Sun and Y.S. Lee, *J. Mater. Chem. A*, 5 (2017) 8408-8415.
11. T.R. Chen, Z.G. Wu, W. Xiang, E.H. Wang, C.J. Wu, M.Z. Chen, X.D. Guo and B.H. Zhong, *Ceram. Int.*, 43 (2017) 6303-6311.
12. C.J. Jafta, M.K. Mathe, N. Manyala, W.D. Roos and K.I. Ozoemena, *ACS Appl. Mater. Interfaces*, 5 (2013) 7592-7598.
13. F.P. Nkosi, K.Raju, N. Palaniyandy, M.V. Reddy, C. Billing and K.I. Ozoemena, *J. Electrochem. Soc.*, 164 (2017) A3362-A3370.
14. P. Manikandan, S. Heo, H.W. Kim, H.Y. Jeong, E. Lee and Y. Kim, *J. Power Sources*, 363 (2017) 442-449.
15. P. Manikandan, H.W. Kim, S. Heo, E. Lee and Y. Kim, *ACS Appl. Mater. Interfaces*, 9 (2017) 10618-10625.
16. Z.Y. Li, R. Gao, L. Sun, Z. Hu and X. Liu, *Electrochim. Acta 223* (2017) 92-99.
17. H. Yoshi, N. Yabuuchi, K. Kubota, I. Ikeuchi, A. Garsuch, M. Schulz-Dobrick, and S. Komaba, *Chem. Commun.*, 50 (2014) 3667-3680.
18. J. Xu, D.H. Lee, R.J. Clement, X. Yu, M. Leskes, A.J. Pell, G. Pintacuda, X.-Q. Yang, C.P. Grey and Y.S. Meng, *Chem. Mater.*, 26 (2014) 1260-1269.
19. K. Kaliyappan, J. Liu, B. Xiao, A. Lushington, R. Li, T.K. Sham and X. Sun, *Adv. Funct. Mater.*, 27 (2017), 1701870.
20. M.J. Aragón, P. Lavela, G. Ortiz, R. Alcántara and J.L. Tirado, *J. Alloys Compd.*, 724 (2017) 465-473.
21. C.J. Jafta, K.I. Ozoemena, M.K. Mathe and W.D. Roos, *Electrochim. Acta*, 85 (2012) 411-422.
22. J.Y. Li, H.Y. Lü, X.H. Zhang, Y.M. Xing, G. Wang, H.Y. Guan and X.L. Wu, *Chem. Eng. J.*, 316 (2017) 499-505.